ISSN 0016-7029, Geochemistry International, 2007, Vol. 45, No. 6, pp. 546–560. © Pleiades Publishing, Ltd., 2007.
Original Russian Text © M.A. Mishkin, A.M. Lennikov, G.M. Vovna, Z.G. Badredinov, R.A. Oktyabr'skii, 2007, published in Geokhimiya, 2007, No. 6, pp. 608–623.

Geochemistry and Protoliths of the Metabasite–Enderbite Association of the Dzhugdzhur Block, Aldan Shield

M. A. Mishkin, A. M. Lennikov, G. M. Vovna, Z. G. Badredinov, and R. A. Oktyabr'skii

Far East Geological Institute, Far East Division, Russian Academy of Sciences,
pr. Stoletiya Vladivostoka 159, Vladivostok, 690022 Russia
e-mail: gala1367@mail.ru

Received November 9, 2005

Abstract—The bottom of the stratigraphic sequence of the Dzhugdzhur deep-seated granulite complex was determined to consist of a stratified metabasite–enderbite association. The distributions of major and trace elements indicate that the protoliths of the association were volcanic rocks of the calc–alkaline, komatiite–tholeiite, and picrite series. The model assumed for the genesis of the protolithic volcanics of the metabasite–enderbite association includes two stages. The first of them was responsible for the decompression-induced partial melting of the material of an ascending mantle plume with the derivation of melts of the komatiite–tholeiite series. During the second stage, the volcanics of the calc–alkaline series were produced by the partial melting of the metabasite crust under the effect of the heat of the ascending mantle plume. The protoliths of the metabasite–enderbite association were formed in the Early Proterozoic.

DOI: 10.1134/S0016702907060031

INTRODUCTION

Earlier petrological studies of the metamorphic complexes of the Aldan Shield have demonstrated that the deepest granulites (of the Sutam depth facies) compose its southern part [1]. These granulites, which include abundant enderbites, are exposed at the surface in a series of tectonic blocks: Sutam, Zverevskii, Kurul'ta, and Dzhugdzhur. Data of mineralogical geothermobarometry indicate that the rocks composing these blocks were metamorphosed at granulite-facies temperatures and pressures of 8–10 kbar [2–4]. This provided grounds to believe that these blocks are fragments of lower crustal levels corresponding to depths of approximately 30 km. Because of this, the granulite complexes of these blocks are particularly interesting for reconstructing the composition of the lower crust in the eastern part of the Asian continent.

Our research was centered on the identification of the protoliths of the granulite complex of the Dzhugdzhur block and their role in the origin of the sialic basement of the eastern Aldan Shield. This publication reports the first data on the geochemistry of granulites of the Dzhugdzhur granulites and their Sm–Nd isotopic systematics.

GEOLOGY

The Dzhugdzhur block is located in the southeastern part of the Aldan Shield, in the basins of the Kun-Man'e, Ayumkan, and Maya rivers (Figs. 1, 2). The stratified nature of the Dzhugdzhur granulites was first demonstrated by Moshkin [8], who subdivided them into two units: lower, consisting of pyroxene–plagioclase crystalline schists and gneisses, and upper, made up of biotite–garnet gneisses with marble beds. The territory of the Dzhugdzhur block was later covered by a 1: 200000 geological survey (under the supervision of Gamaleya [9]). Gamaleya proposed a further stratigraphic subdivision of the Archean metamorphic sequences into four conformable formations (from bottom to top): Upper Sunnagin, Kyurikan, Sutam, and Khudurkan. Based on the analysis of literature data and our own field observations, the authors of this paper consider it expedient to return to Moshkin's scheme [8], according to which the Dzhugdzhur metamorphic complex is subdivided into two units. The lower one consists of hypersthene plagiogneisses (enderbites) intercalating with clinopyroxene–orthopyroxene schists. The upper unit is dominated by biotite–garnet, biotite, and biotite–graphite gneisses with marble beds and subordinate enderbites and pyroxene–biotite gneisses. The distribution of these units within the study area is shown in Fig. 2. The lower unit represents early stages in the crustal evolution of the southeastern Aldan Shield and was recognized as the metabasite–enderbite association. This publication is devoted to the description of this association.

The enderbites volumetrically dominating in this association are fine- to medium-grained dark gray greenish rocks, whose banding is accentuated by melanocratic bands enriched in hypersthene and, locally, also in hornblende. The lower unit is mostly stratified and includes lenses and beds of metabasites (up to 30% of the unit by volume) and, more rarely, metaultrabasites (up to 5% by volume). The occurrence of these

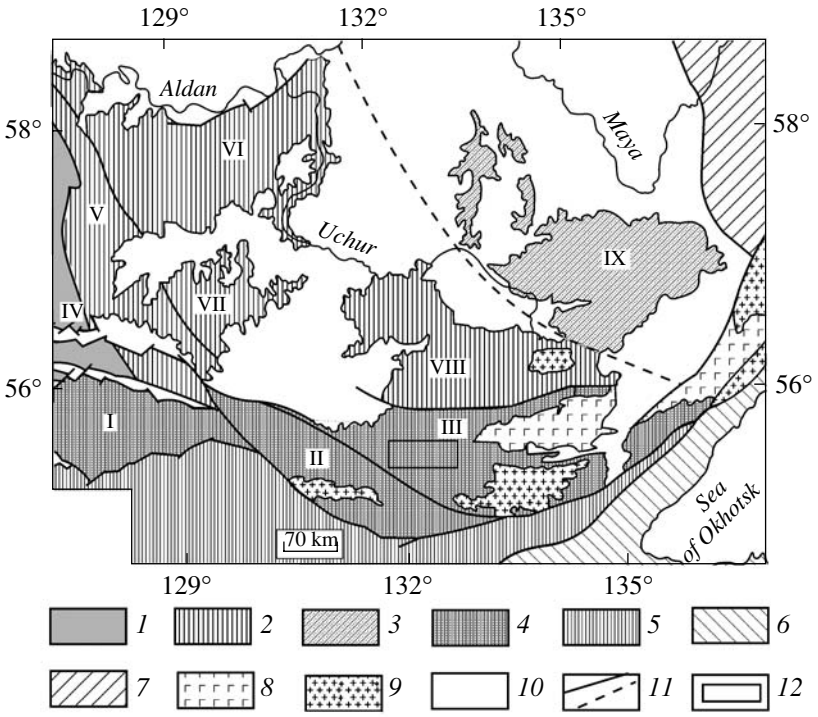

Fig. 1. Schematic tectonic map of the eastern part of the Aldan Shield (simplified after [5]).

(*1–4*) Aldan Shield: (*1*) Western Aldan megablock, (*2*) Eastern Aldan megablock, (*3*) Batomgskii granite–greenstone terrane, (*4*) Southern Aldan geoblock; (*5*) Stanovoi folded area; (*6*) Mongolia–Okhotsk foldbelt; (*7*) Verkhoyansk–Chukot foldbelt; (*8*) anorthosites; (*9*) Phanerozoic granitoids; (*10*) Cenozoic deposits; (*11*) faults; (*12*) study area.

Roman numerals denote blocks: (I) Sutam, (II) Ayumkan, (III) Dzhugdzhur, (IV) Nimnyrskii, (V) Kholbolokhskii, (VI) Sunnagin, (VII) Gonam, (VIII) Tyrkan, (IX) Botomgskii.

rocks suggests that the protoliths of the unit were essentially volcanic, unlike those of the upper unit, whose marbles and graphite–biotite schists testify that its protoliths contained much sedimentary rocks. The rock-forming minerals of the enderbites are antiperthitic plagioclase (50–70%, 40–50% *An*), quartz (5–10%), hypersthene (5–10%), hornblende (8–10%), magnetite (up to 7%), clinopyroxene (up to 5%), and rare biotite flakes. The accessory minerals are apatite, zircon, ilmenite, rutile, and pyrite.

The clinopyroxene–orthopyroxene schists consist of plagioclase (30–40%, 50–58% *An*), clinopyroxene (20–40%), and orthopyroxene (5–10%). Some varieties of the orthopyroxene–clinopyroxene schists contain minor amounts of garnet or biotite. The accessory minerals are apatite, zircon, titanomagnetite, and ilmenite.

The ultrabasic crystalline schists (orthopyroxene–clinopyroxene, orthopyroxene–clinopyroxene–amphibole, and olivine–orthopyroxene–clinopyroxene–amphibole) are massive rocks consisting of orthopyroxene (10–35%), clinopyroxene (10–45%), olivine (0–19%), and amphibole (0–80%) with minor amounts of ilmenite, and, sometimes, biotite and spinel.

According to the results of mineralogical geothermobarometry, the rocks of the Dzhugdzhur block were metamorphosed to the granulite facies at a maximum temperature of 800°C and pressure of 9 kbar [3].

The age of the Dzhugdzhur Complex is provisionally assumed to be Archean, although this was not confirmed by isotopic dating. It was determined that the anorthosites of the Dzhugdzhur Massif intrude the granulites of the Dzhugdzhur Complex [10]. The age of the Dzhugdzhur anorthosites is also disputable. For example, the Pb isochron method yielded age values of the anorthosites ranging from 2.7 [11] to 1.734–1.736 Ga [12], and two mineral Sm–Nd isochrons corresponded to 1702 ± 27 Ma and 1705 ± 30 Ma [10]. We obtained the first data on the Sm–Nd isotopic systematics of the rocks of the metabasite–enderbite association of the Dzhugdzhur Complex that testify to its Early Proterozoic age.

GEOCHEMISTRY OF THE GRANULITES AND THEIR PROTOLITHS

Rocks from the Dzhugdzhur Complex were analyzed for major elements at the Far East Geological Institute, Far East Division, Russian Academy of Sciences, by conventional chemical techniques (analyst L.V. Nedashkovskaya). Trace elements were deter-

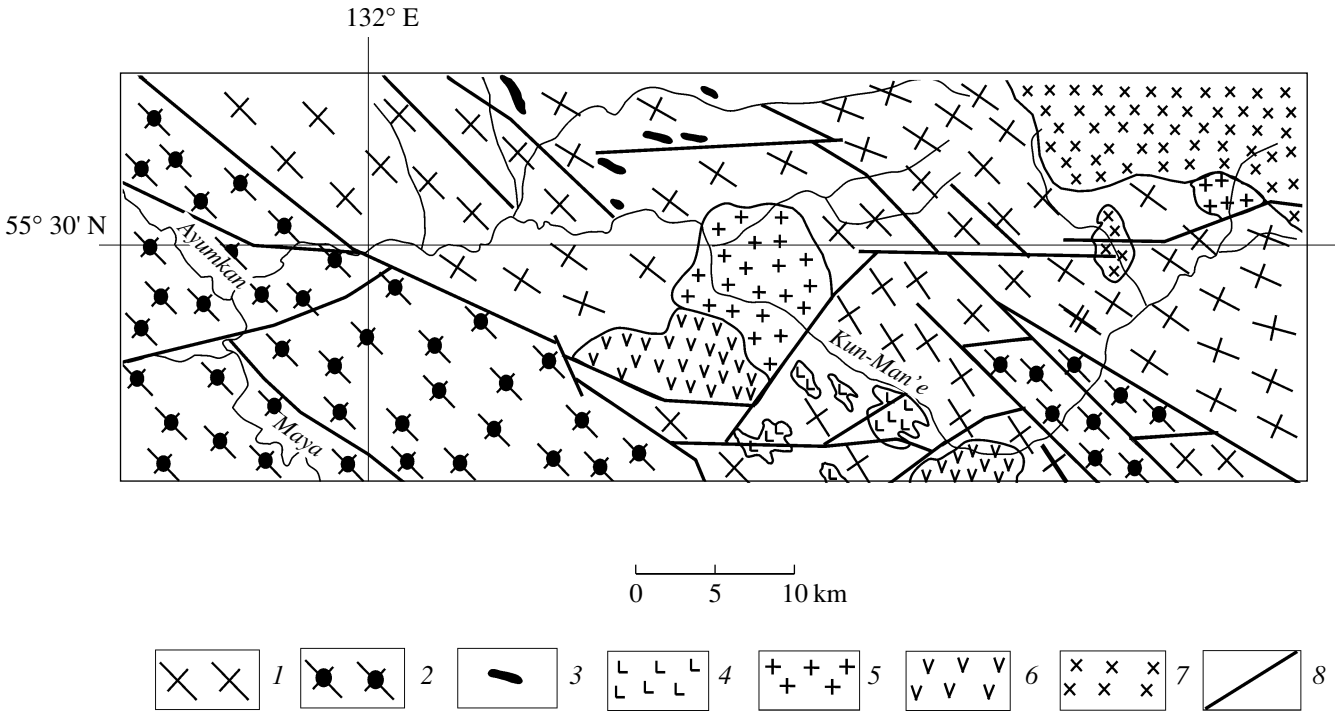

Fig. 2. Schematic geological map of the study area (modified after a Geological Map of the USSR, scale 1 : 200000, sheets N-53-I and N-52-IV [6, 7], with the use of the field observations and data of A.M. Lennikov, P.A. Oktyabrskii, and M.A. Mishkin).
(*1*, *2*) Dzhugdzhur granulite complex: (*1*) granulites of the lower unit (enderbites and metabasites); (*2*) granulites of the upper unit (aluminous gneisses, enderbites, metabasites, and calciphyres); (*3–5*) Early Proterozoic metaintrusive rocks: (*3*) 3meta hyperbasites and basites, (*4*) anorthosites, (*5*) granites; (*6*) rocks of the platform cover; (*7*) Cretaceous granites; (*8*) faults.

mined by ICP-MS at the Laboratory of Isotopic Research of the Vinogradov Institute of Geochemistry, Siberian Division, Russian Academy of Sciences, in Irkutsk. The Sm–Nd determinations were carried out by G.M. Vovna on Finnigan MAT-262 under the supervision of Prof. D. Maeda at the Hokkaido University in Sapporo, Japan. The data on the chemical composition of rocks of the metabasite–enderbite association of the Dzhugdzhur Complex are based on analyses of 52 samples, which represent rocks not affected by migmatization. Representative analyses of rocks of the metabasite–enderbite association are listed in Tables 1 and 2.

The original composition of the metamorphic rocks was reconstructed based on the materials of field structural observations and the analysis of petrochemical data and the distributions of trace elements in the rocks.

Statistical literature data on the chemical variations in rocks metamorphosed to the amphibolite and granulite facies inclusive highlight the relatively immobile behavior of major elements (except alkalis). This warrants the application of petrochemical diagrams with the purpose of reconstructing the protoliths of metamorphic rocks. This does not, however, pertain to rocks affected by migmatization or other metasomatic transformations.

The geochemical behavior of trace elements during granulite metamorphism was examined by many researchers. Granulites are known to be depleted in some lithophile elements, such as Rb, U, and Th [13], while Ba and Sr show features of a mobile behavior. It is also thought that REE are relatively inert during granulite-facies metamorphism (except Eu [14]). Some researchers admit the possibility of a mobile behavior of LREE [15], but this issue is still largely obscure and can be explained by the possible effect of metasomatic processes. HFSE (Ti, Nb, Y, Zr, Hf, and Ta) are inert during metamorphism, as also are ferrophile elements (Ni, Co, and Cr) [15].

It is known that, when the protoliths of metamorphic rocks are reconstructed, it is particularly difficult to do this for rocks of intermediate and acid composition, for which uncertainties often arise in ascribing them to magmatic or sedimentary rocks.

In order to resolve this problem, Dennen and Moor [16] proposed a discriminant diagram (Fig. 3), in which the hypersthene plagiogneisses of intermediate composition of the Dzhugdzhur metabasite–enderbite association plot in the field of magmatic rocks.

In the $Na_2O + K_2O$-SiO_2 classification plot (Fig. 4) for volcanic rocks [17], the compositions of the granulites of the metabasite–enderbite association cluster mostly within fields of normal alkalinity (from ultrabasic rocks to andesites).

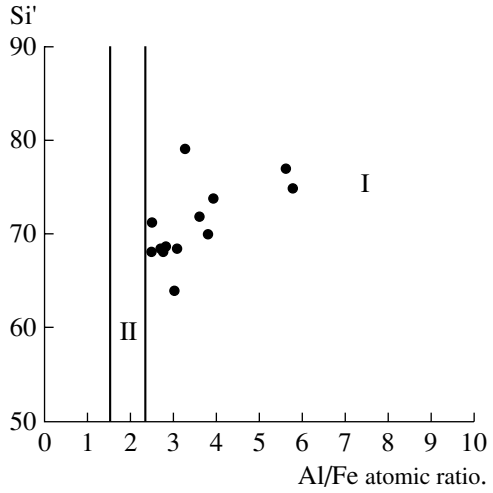

Fig. 3. Petrochemical diagram for distinguishing between ortho- and paragneisses (after [16]), Si' = Si/(Si + Fe + Al) × 100.
Data points correspond to the compositions of granulites of the Dzhugdzhur Complex. Fields: (I) magmatic rocks; (II) sedimentary rocks.

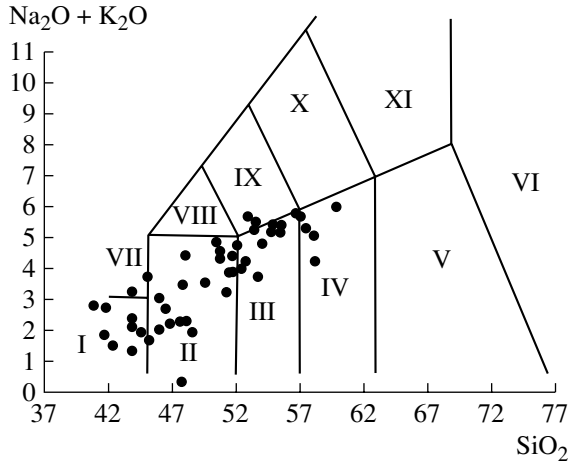

Fig. 4. SiO_2–(Na_2O + K_2O) classification diagram [17] for orthorocks of the Dzhugdzhur granulite complex.
Roman numerals denote rock fields: (I) picrobasalts, (II) basalts, (III) basaltic andesites, (IV) andesites, (V) dacites, (VI) rhyolites, (VII) basanites, (VIII) trachybasalts, (IX) basaltic trachyandesites; (X) trachyandesites, (XI) trachydacites.

These interpretations of the protoliths of the granulites are corroborated by the SiO_2–Ca/Mg–Fe_{tot}/(Ca + Mg + Fe_{tot}) diagram [18] (Fig. 5) and by the diagram [19] (Fig. 6), in which the ratio of Zr to Ti (the most inert major component) is taken into account, which is particularly important when the protoliths of granulite-facies rocks are reconstructed. In the Al–(Fe + Ti)–Mg classification diagram [20] (Fig. 7), the granulites plot within the fields of volcanics of the calc–alkaline and komatiite–tholeiite series.

Metavolcanic Rocks of the Calc–Alkaline Series

The volcanics of this series include metamorphosed basalts, basaltic andesites (orthopyroxene–clinopyroxene schists), and andesites (enderbites). Because of this

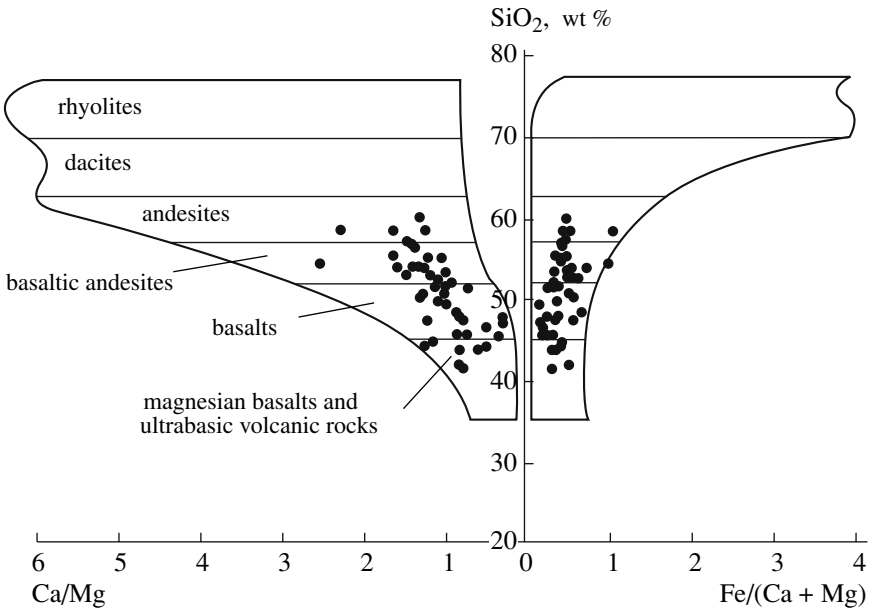

Fig. 5. Classification petrochemical diagram for volcanic rocks [18]. Circles correspond to the compositions of rocks from the Dzhugdzhur Complex.

Table 1. Chemical composition of metabasites and enderbites of the protolithic basalt–andesite association

Component	E-24/222	E-14/136	E-37/318	E-17/159	E-17/177	E-25/238	E-16/148	E-17/163	E-17/165	E-17/164	E-33/285	E-17/158	E-35/296	E-17/171	E-17/168	E-36/312	E-42/343	E-17/156
	1	2	3	4	5	6	7	8	9	10	11	12	13	14	15	16	17	18
	Orthopyroxene–clinopyroxene crystalline schists														*Hypersthene plagiogneisses*			
SiO_2	45.02	50.88	51.99	53.01	53.59	53.48	53.86	54.67	54.8	54.88	55.31	55.58	56.74	56.83	57.41	58.22	58.19	59.78
TiO_2	0.75	0.71	0.84	0.84	1.07	0.69	0.7	0.61	0.55	0.7	0.42	0.49	0.59	0.69	0.7	0.68	0.69	0.59
Al_2O_3	20.91	17.1	16.78	18.25	18.1	18.95	17.39	17.19	17.26	17.62	19.5	18.14	18.25	16.61	16.83	16.09	16.28	17.06
Fe_2O_3	5.83	2.11	2.84	4.99	4.35	4.59	4.03	2.98	2.75	4.1	2.45	4.64	4.73	3.32	3.61	1.28	3.65	2.61
FeO	6.37	7.1	6.7	4.65	4.93	4.83	5.79	5.63	5.83	4.66	4.17	3.82	2.8	4.71	4.51	6.98	5.21	4.12
MnO	0.1	0.12	0.13	0.17	0.17	0.15	0.15	0.15	0.17	0.14	0.09	0.14	0.1	0.14	0.16	0.12	0.15	0.13
MgO	6.54	7.04	6.59	3.78	3.92	3.95	4.74	5.2	4.61	4.32	3.72	4	3.45	4.27	3.93	3.77	4.03	3.16
CaO	9.63	9.12	9.51	7.55	7.53	7.36	7.68	7.46	7.62	7	8.3	7.33	6.96	7.3	6.65	6.44	6.84	5.74
Na_2O	2.67	3.32	2.75	4.4	4.3	4.22	4.0	3.81	3.84	4.01	4.27	4.12	4.66	3.7	3.4	3.6	3.65	4.25
K_2O	1.03	1.03	0.61	1.26	0.98	1.33	0.85	1.35	1.61	1.12	1.13	1.06	1.12	2.02	1.91	1.52	0.58	1.75
P_2O_5	0.18	0.29	0.41	0.49	0.52	0.38	0.3	0.33	0.32	0.32	0.33	0.26	0.29	0.41	0.27	0.31	0.31	0.36
LOI	0.97	1.18	0.85	0.61	0.54	0.07	0.51	0.62	0.64	1.13	0.31	0.42	0.31	0	0.62	0.99	0.42	0.45
U	0.18	0.25	0.04	0.03	–	–	0.02	–	0.02	0.03	0.07	0.02	–	0.01	0.01	0.75	0.03	0.01
Th	0.58	0.86	0.28	0.12	–	–	0.06	–	0.09	0.26	0.43	0.09	–	0.03	0.26	3.22	0.08	0.04
Ba	310.93	225.66	410.58	398.66	–	–	413.21	–	490.56	692.03	856.76	544.95	–	838.12	685.77	339.44	286.11	700.21
Sr	939.3	268	483.38	976.86	–	–	586.7	–	758.69	822.75	870.58	911.86	–	718.98	715.94	594.24	555.65	712.35
La	12.56	14.56	18.27	34.86	–	–	17.2	–	19.22	21.12	20.99	20.67	–	24.08	17.37	33.44	11.57	20.5
Ce	25.42	34.03	41.27	78.77	–	–	37.23	–	41.73	46.57	41.87	45.65	–	58.02	40.53	70.28	24.82	44.01
Pr	3.32	4.68	5.65	10.06	–	–	5.07	–	5.62	6.52	5.36	6.19	–	7.85	5.63	8.86	3.41	5.9

Table 1. (Contd.)

Component	E-24/222	E-14/136	E-37/318	E-17/159	E-17/177	E-25/238	E-16/148	E-17/163	E-17/165	E-17/164	E-33/285	E-17/158	E-35/296	E-17/171	E-17/168	E-36/312	E-42/343	E-17/156
	1	2	3	4	5	6	7	8	9	10	11	12	13	14	15	16	17	18
	Orthopyroxene–clinopyroxene crystalline schists														*Hypersthene plagiogneisses*			
Nd	12.7	19.32	22.99	40.77	–	–	21.23	–	23.54	27.42	22.5	26.12	–	33.13	23.41	34.8	13.83	24.78
Sm	2.44	4.31	4.55	7.41	–	–	4.47	–	4.69	5.45	4.57	5.27	–	6.4	4.76	6.39	2.74	4.93
Eu	1.02	1.2	1.45	2.14	–	–	1.6	–	1.38	1.61	3.58	1.34	–	1.54	1.07	1.39	1	1.35
Gd	2.23	4.34	4.53	6.06	–	–	3.96	–	4.14	4.87	4.4	4.83	–	5.47	4.27	5.85	2.85	4.34
Tb	0.33	0.7	0.72	0.96	–	–	0.59	–	0.65	0.81	0.71	0.76	–	0.9	0.7	0.94	0.47	0.72
Dy	1.55	3.7	3.68	3.96	–	–	2.88	–	3.22	3.86	3.66	3.8	–	4.23	3.35	4.46	2.51	3.63
Ho	0.29	0.77	0.75	0.78	–	–	0.58	–	0.66	0.79	0.74	0.75	–	0.88	0.69	0.87	0.51	0.76
Er	0.82	2.27	2.18	2.32	–	–	1.72	–	1.95	2.3	2.11	2.21	–	2.56	2.04	2.49	1.52	2.19
Tm	0.1	0.31	0.29	0.3	–	–	0.22	–	0.28	0.33	0.3	0.32	–	0.37	0.29	0.34	0.22	0.32
Yb	0.69	2.02	1.86	1.79	–	–	1.5	–	1.79	2.03	1.82	2.09	–	2.35	1.87	2.16	1.45	2.06
Lu	0.1	0.29	0.27	0.29	–	–	0.23	–	0.27	0.31	0.27	0.3	–	0.36	0.28	0.32	0.23	0.31
Zr	25.4	41.76	49.04	29.01	–	–	17.33	–	34.32	25.51	40.79	21.1	–	34.08	26.3	22.68	49.7	25.07
Hf	0.73	1.35	1.32	0.98	–	–	0.7	–	1.12	1.01	1.12	0.84	–	1.13	0.89	0.88	0.24	0.96
Ta	0.61	0.38	0.39	0.64	–	–	0.3	–	0.5	0.39	0.45	0.26	–	0.34	0.51	0.85	0.31	0.44
Nb	3.25	5.18	5.27	12.16	–	–	5.2	–	4.82	6.81	3.17	4.53	–	6.76	6.26	16.54	5.54	6.23
Y	7.15	18.48	18.23	19.43	–	–	14.96	–	15.97	18.88	16.99	16.8	–	21.14	15.42	21.03	12.34	18.49
Sc	18.92	28.44	25.46	18.53	–	–	20.46	–	22.23	24.32	23.31	21.86	–	21.78	19.69	17.71	20.19	19.39
Ni	27.69	34.86	62.59	20.25	–	–	21.79	–	45.36	30.91	47.12	26	–	39.16	36.84	58.35	25.3	21.55
Co	52.14	37.95	36.83	25.86	–	–	29.46	–	28.35	26.96	22.85	24.29	–	25.66	23.64	20.91	21.59	21.39
V	310.37	201.08	137.37	151.08	–	–	150.16	–	164.74	192.92	151.64	158.59	–	121.48	159.70	179.89	83.80	141.20

Note: Oxides are given in wt %, trace elements are in ppm. All analyses are normalized to 100 wt % major oxides; dashes mean not analyzed. Rocks: (1–3) metabasalts; (4–14) metamorphosed basaltic andesites; (15–18) metaandesites.

Table 2. Chemical composition of basic and ultrabasic volcanic rocks of the Dzhugdzhur Complex

Component	E-13/104	E-14/119	E-17/162	E-14/121	E-25/237	E-10/77	2107-A	E-14/134	E-35/301	E-17/174	E-17/160	E-14/117	E-7/66	E-17/175	E-37/313	E-37/319	E-32/284	E-40/337	E-14/126	
	1	2	3	4	5	6	7	8	9	10	11	12	13	14	15	16	17	18	19	20
	Orthopyroxene–clinopyroxene crystalline schists																			
SiO_2	42.10	42.43	43.84	43.86	44.2	44.66	45.70	46.06	46.06	46.61	46.92	47.73	48.56	48.04	50.34	50.72	51.65	52.29	53.9	49.83
TiO_2	1.01	0.45	1.55	0.46	1.11	1.23	0.58	0.65	1.23	0.66	0.72	1.56	0.25	1.01	1.94	2	0.94	0.85	0.45	1.65
Al_2O_3	14.67	12.74	12.06	13.63	14.78	12.79	9.16	8.45	8.39	8.84	8.00	13.02	2.82	16.20	14.5	15.44	15.79	14.02	14.53	13.98
Fe_2O_3	6.61	4.89	5.83	3.55	5.73	5.85	1.29	1.01	4.15	5.23	4.66	4.11	2.54	4.24	1.6	3.78	2.45	3.09	2.7	5.00
FeO	6.90	13.59	8.12	14.35	8.67	9.7	9.97	11.19	11.38	6.95	6.53	12.15	9.49	7.66	11.04	8.58	7.45	7.54	7.33	10.09
MnO	0.17	0.22	0.16	0.20	0.14	0.96	0.25	0.17	0.23	0.17	0.17	0.23	0.24	0.14	0.16	0.14	0.13	0.16	0.17	0.22
MgO	11.17	9.91	13.11	9.81	10.78	8.22	22.10	11.53	13.1	17.39	24.30	6.65	27.64	9.18	5.09	5.18	7.35	8.02	7.12	6.31
CaO	10.92	10.31	9.46	8.99	11.11	13.22	8.13	12.4	11.84	10.13	5.57	10.57	6.48	9.00	8.64	8.58	9.34	9.35	8.99	9.72
Na_2O	2.20	0.40	2.33	0.66	2.10	1.70	1.30	1.00	1.48	1.92	1.15	1.97	0.34	2.59	3.63	3.37	3.18	3.18	3.3	2.53
K_2O	0.59	1.15	0.93	1.47	0.24	0.22	0.20	2.01	0.58	0.80	1.06	0.33	0.01	0.89	1.24	1.22	0.72	0.84	0.47	0.38
P_2O_5	0.50	0.99	0.21	0.45	0.19	0.39	0.12	2.65	0.31	0.24	0.0	0.25	0.07	0.21	0.68	0.87	0.24	0.31	0.24	0.25
LOI	3.16	2.92	2.4	2.57	0.95	1.06	1.20	2.88	1.25	1.06	0.82	1.43	1.56	0.84	1.14	0.12	0.76	0.35	0.8	0.05
U	0.09	–	–	–	0.12	0.14	0.42	0.47	0.09	<0.02	0.02	–	<0.02	0.04	–	0.1	<0.02	0.23	0.03	–
Th	0.41	–	–	–	0.28	0.38	0.64	3.92	0.43	0.18	0.26	–	0.12	0.24	–	0.79	0.12	1.15	0.3	–
Ba	355.86	–	–	–	150.04	34.43	<10	3755.29	222.70	76.46	237.99	–	<10	365.10	–	821.96	482	134.04	177	199.0
Sr	520.50	–	–	–	878.07	146.7	55.21	1053.16	386.05	171.11	163.58	–	21.54	618.03	–	515.44	587.86	358.42	288.67	150.0
La	33.57	–	–	–	9.50	12.67	2.84	151.81	13.01	6.83	21.58	–	1.81	12.97	–	56.71	14.02	40.02	10.29	8.63
Ce	74.13	–	–	–	22.03	36.58	7.30	359.25	37.48	22.46	60.18	–	5.37	34.81	–	122.15	29.73	95.19	26.23	20.3
Pr	9.91	–	–	–	3.23	5.37	1.06	49.68	6.33	3.87	8.27	–	0.86	5.64	–	15.62	4.14	12.66	4.11	–
Nd	41.49	–	–	–	14.12	23.33	4.94	202.04	29.4	17.95	31.02	–	4.29	25.7	–	63.55	17.71	49.71	17.19	13.8
Sm	8.54	–	–	–	3.22	5.95	1.50	29.81	7.17	3.99	4.85	–	1.26	5.87	–	12.09	3.87	9.23	3.74	4.2
Eu	2.36	–	–	–	1.15	1.64	0.71	5.62	1.55	1.18	1.13	–	0.36	1.69	–	3.06	1.64	2.29	1.08	1.4

Table 2. (Contd.)

Component	E-13/104	E-14/119	E-17/162	E-14/121	E-25/237	E-10/77	2107-A	E-14/134	E-35/301	E-17/174	E-17/160	E-14/117	E-7/66	E-17/175	E-37/313	E-37/319	E-32/284	E-40/337	E-14/126	
	1	2	3	4	5	6	7	8	9	10	11	12	13	14	15	16	17	18	19	20
	Orthopyroxene–clinopyroxene crystalline schists																			
Gd	8.14	–	–	–	3.24	6.59	2.09	17.96	7.48	4.08	4.08	–	1.45	5.72	–	11.32	3.82	7.42	3.67	–
Tb	1.18	–	–	–	0.48	1.16	0.36	2.23	1.13	0.59	0.58	–	0.22	0.88	–	1.77	0.62	1.04	0.6	0.95
Dy	6.01	–	–	–	2.28	7.06	2.15	6.21	5.84	3.17	2.28	–	1.27	4.39	–	7.83	3.21	4.35	3.19	–
Ho	1.28	–	–	–	0.41	1.58	0.46	0.96	1.17	0.64	0.42	–	0.26	0.87	–	1.55	0.66	0.75	0.66	–
Er	3.85	–	–	–	1.12	4.95	1.32	n.d.	3.42	1.84	1.27	–	0.75	2.48	–	4.6	1.97	2.25	1.92	–
Tm	0.51	–	–	–	0.13	0.73	0.18	0.28	0.45	0.24	0.14	–	0.1	0.31	–	0.58	0.26	0.26	0.27	–
Yb	3.38	–	–	–	0.80	4.81	1.18	1.92	2.87	1.56	0.92	–	0.66	1.99	–	3.62	1.67	1.64	1.76	3.1
Lu	0.52	–	–	–	0.11	0.74	0.18	0.27	0.41	0.22	0.13	–	0.1	0.28	–	0.51	0.25	0.23	0.27	0.46
Zr	37.89	–	–	–	29.38	83.04	36.91	29.48	70.74	43.3	62.99	–	10.63	54.88	–	55.52	44.43	18.85	44.0	94.33
Hf	1.17	–	–	–	0.88	2.07	1.06	1.28	2.38	1.38	1.57	–	0.4	1.64	–	2.06	1.24	0.93	1.45	–
Ta	0.33	–	–	–	0.32	0.52	<0.2	0.55	0.35	<0.2	0.25	–	<0.2	0.52	–	0.95	0.43	0.56	<0.2	–
Nb	5.36	–	–	–	3.00	8.75	1.39	12.09	6.50	3.57	4.52	–	0.25	4.97	–	21.35	6.61	10.47	1.98	6.1
Y	32.61	–	–	–	10.00	40.04	10.53	25.04	30.04	15.45	9.34	–	6.44	20.35	–	39.9	16.36	19.14	16.15	29.66
Sc	33.63	–	–	–	32.75	56.46	31.81	25.95	53.84	52.32	30.29	–	30.38	42.08	–	28.98	31.57	34.31	33.34	–
Ni	193.27	–	–	–	144.06	122.79	845.46	25.95	145.01	120.2	431.12	–	645.31	107.22	–	30.8	70.61	232.2	25.36	–
Co	49.64	–	–	–	78.06	58.12	85.05	25.23	76.73	76.81	96.98	–	104.12	54.1	–	34.51	46.45	51.53	35.65	–
V	268.93	–	–	–	315.35	377.23	186.63	167.78	361.02	196.1	137.27	–	105.16	283.5	–	210.99	160.81	206.51	137.13	–
Al_2O_3/TiO_2	14.52	28.31	7.78	29.63	13.32	10.40	10.75	13.00	6.82	13.39	11.11	8.35	12.96	16.04	7.47	7.72	16.80	16.49	32.29	8.47
CaO/TiO_2	10.81	22.91	6.10	19.54	10.01	10.75	11.71	19.08	9.63	15.35	7.74	6.78	26.43	8.91	4.45	4.29	9.94	11.00	19.98	5.89
CaO/Al_2O_3	0.74	0.81	0.78	0.66	0.75	1.03	1.09	1.47	1.41	1.15	0.70	0.81	2.04	0.56	0.60	0.56	0.59	0.67	0.62	0.70

Note: Oxides are given in wt %, trace elements are in ppm. All analyses are normalized to 100 wt % major oxides; dashes mean not analyzed. Rocks: (1–5, 8, 10, 14) komatiite metabasalts, (9, 16) picrite metabasalts, (6, 12, 15–19) tholeiite metabasalts, (7, 11, 13) metakomatiites, (20) average composition of the tholeiite metabasalt of the Sutam granulite complex.

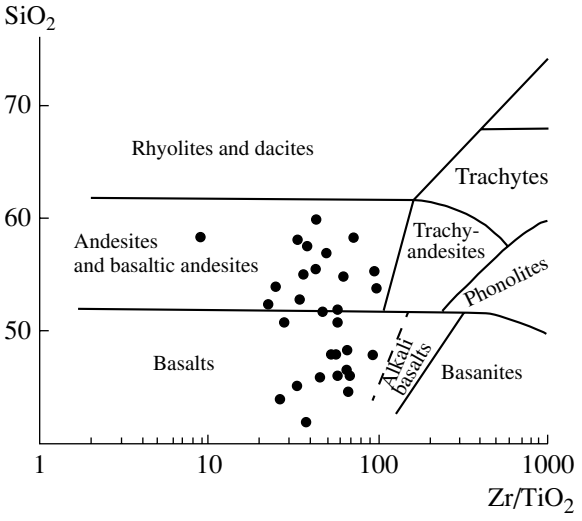

Fig. 6. SiO_2–Zr/TiO_2 diagram [19] for the granulites of the Dzhugdzhur Complex. Circles correspond to the compositions of rocks from the Dzhugdzhur Complex.

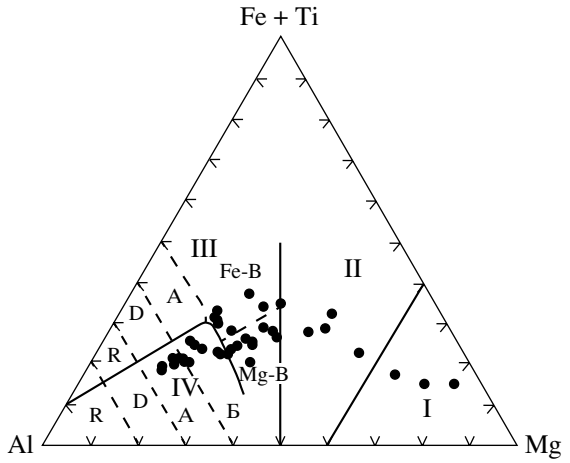

Fig. 7. Al–Fe + Ti–Mg classification diagram [20]. Circles correspond to the compositions of granulites from the Dzhugdzhur Complex. Roman numerals denote compositional fields: (I) komatiites, (II) komatiite and high-Mg basalts, (III, IV) volcanic rocks of the tholeiite and calc–alkaline series, respectively. Letters denote fields: R—rhyolites; D—dacites; A—andesites; B—basalts (Fe-B and Mg-B are high-Fe and high-Mg basalts, respectively).

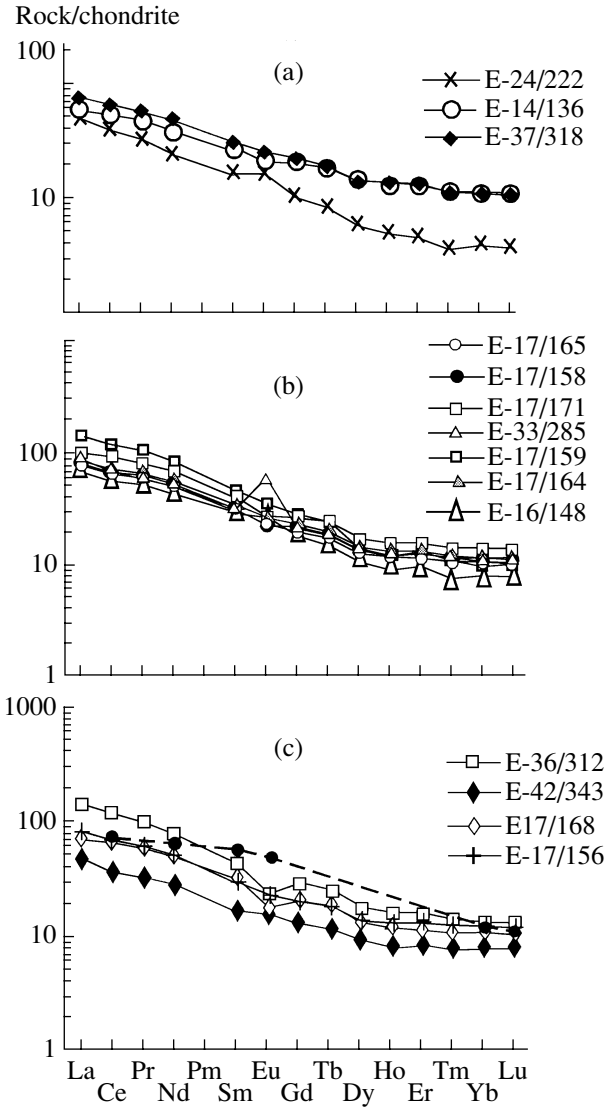

Fig. 8. Chondrite-normalized [21] REE patterns for the metavolcanic rocks of the basalt–andesite association of the calc–alkaline series of the Dzhugdzhur granulite complex. (a) Metabasalts, (b) metamorphosed basaltic andesites, (c) metaandesites. The dashed line with solid circles in Fig. 8c shows the REE pattern of the model andesite melt.

the metavolcanics of the calc–alkaline series were recognized as a basalt–andesite association. Representative analyses of rocks of this association are given in Table 1. The metamorphosed basalts and basaltic andesites belong to the aluminous type ($A1_2O_3$ > 15 wt %). The REE patterns of the metabasalts correspond to those of Archean basalts of TH2 [22] (Fig. 8a). They are characterized by mild enrichment in LREE, $(La/Yb)_N$ = 12.68–6.63. A similar topology of REE patterns is typical of the basaltic andesites, which differ by slightly elevated concentrations of LREE (Fig. 8b).

The REE patterns of the metaandesites correspond to those of Archean andesites of group II, according to Condie [22], and are characterized by weak REE differentiation [$(La/Yb)_N$ = 5–13] and low Eu anomalies (Fig. 8c).

In a multielement diagram (Fig. 9), the metaandesites of the protolithic basalt–andesite association show concentrations of lithophile elements (except Zr) higher than those in the andesites of the Kurile–Kamchatka island arc [23] and are thus similar to Archean gray gneisses in the basements of shields [24].

The parental melts of the "gray-gneiss" sialic crust are often thought to have been derived by the partial melting of mafic sources, and this idea was confirmed by the results of numerous experiments.

It was demonstrated above that the REE patterns of the Dzhugdzhur metaandesites are depleted in HREE. This suggests that the parental andesite melt was in equilibrium with a garnet-bearing residue.

Available experimental data on the melting of basic rocks indicate that the minimum pressure under which the residue of the melting metabasite contains garnet is equal to 10 kbar [26]. In the experiment of the aforementioned authors, melts with 58% SiO_2 (average silicity of the metaandesites of the Dzhugdzhur Complex) should have been derived at $T = 975°C$ and a degree of partial melting equal to 40%. The residues should have consisted of (vol %) 15% garnet, 1% orthopyroxene, 2% amphibole, 40% clinopyroxene, and 2% plagioclase. Using these data and the REE concentrations in the rocks, it is possible to calculate the composition of the model andesitic melt on the basis of the broadly known relation [27] for the dependence of the concentration of a trace element in a melt on the initial concentration of this element in the source, degree of melting, and the bulk distribution coefficient between the residue phases and melt. It is assumed that the source of the parental andesitic melts of the Dzhugdzhur Complex consisted of tholeiite basalts produced during earlier magmatic events in the southern part of the Aldan Shield. These events could be the formation of the basite protoliths of the granulite complex in the adjacent Sutam block at 3.1 Ga. The average composition of metabasalts in the Sutam block was assumed, according to [28] (Table 2, analysis 20), as the magmatic source from which the andesitic melts of the Dzhugdzhur Complex were derived. The calculation results (Fig. 8c) show good agreement between the compositions of the model melt and natural rocks.

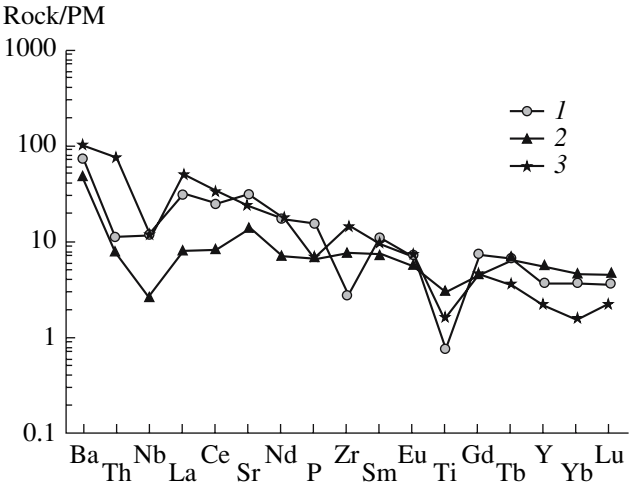

Fig. 9. Multielement diagram normalized to the primitive mantle [25] for metaandesites of the basalt–andesite association. (*1*) Metaandesites of the Dzhugdzhur Complex; (*2*) andesite of the Kurile–Kamchatka island arc [23]; (*3*) composition of Archean gray gneisses [24].

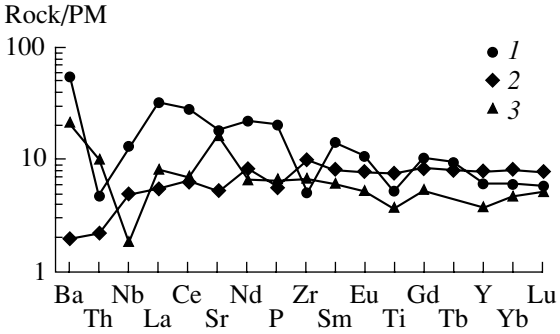

Fig. 10. Multielement pattern normalized to the primitive mantle [25] for (*1*) orthopyroxene–clinopyroxene schists of the Dzhugdzhur Complex; for comparison the diagram also shows the patterns of (*2*) N-MORB tholeiites and (*3*) the basalt of the Kurile island arc.

Metavolcanics of the Komatiite–Tholeiite Series

The protolithic volcanics of this series were determined to have consisted of tholeiite and komatiite basalts and komatiites (komatiite–tholeiite association).

Tholeiite metabasalts

Representative analyses of the tholeiitic metabasalts (orthopyroxene–clinopyroxene schists) are given in Table 2. The MgO concentrations of the tholeiitic metabasalts vary from 4.74 to 10.69 (Table 2, analyses 15–19) at Mg# = 0.58–0.63. A decrease in the MgO contents in the rocks is associated with a decrease in the concentrations of CaO and an increase in Al_2O_3. Consequently, the CaO/Al_2O_3 and CaO/TiO_2 ratios decrease and are lower than the chondritic ones: 0.6 and 12.8, respectively. An increase in the $A1_2O_3$ concentration results in an increase in the Al_2O_3/TiO_2 ratio, whose average value for the tholeiitic metabasalts is 20.62, i.e., is close to the chondritic one. The tholeiitic metabasalts are characterized by moderately differentiated REE patterns [$(La/Yb)_N$) = 4–8] at an approximately 50 times higher concentration of LREE than in chondrites (Fig. 12c). In the multielement diagram of Fig. 10, the metatholeiites of the metabasite–enderbite association differ from N-MORB tholeiitic basalts [29] and the tholeiitic basalts of the Kurile island arc [30] in having elevated contents of Ba, Nb, La, Ce, Nd, and P, which likely indirectly characterizes the geochemistry of the regional crust-forming mantle.

High-Mg Schists of Basic and Ultrabasic Composition

The highly magnesian schists (orthopyroxene–clinopyroxene–olivine and orthopyroxene–clinopyroxene–amphibole) account for approximately 5% of the lower unit by volume. They commonly occur as rela-

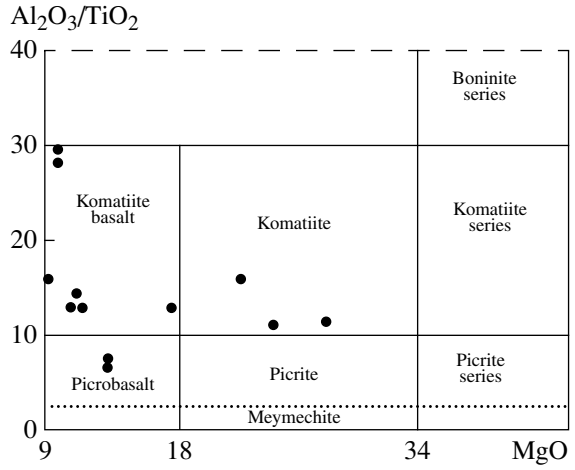

Fig. 11. Discriminant diagram for ultrabasic volcanic rocks of the Dzhugdzhur Complex [31].

tively thin (no thicker than 10 m, occasionally up to a few dozen meters) beds and lenses, which are conformable with the banding of the host enderbites. This suggests that the protoliths of these rocks were of volcanic genesis. Conceivably, some of these beds could originally be sills. Representative analyses of the high-Mg basic and ultrabasic schists are listed in Table 2. In the Al_2O_3/TiO_2–MgO classification diagram [31] (Fig. 11), the high-Mg schists of basic and ultrabasic composition of the Dzhugdzhur Complex plot within the compositional fields of komatiites and komatiite basalts of the komatiite series and in the field of the basalts of the picrite series. The metavolcanics of komatiite and komatiite–basalt composition can also be recognized in the Jensen's classification plot [20], which was discussed above (Fig. 7).

Metakomatiites

The metakomatiites of the Dzhugdzhur Complex meet the conditions specified in the international classification of magmatic rocks [17]: their MgO concentrations are higher than 18 wt % (22.16–27.6 wt %), and the TiO_2 content is lower than 1 wt % (0.25–0.72 wt %) (Table 2, analyses 7, 11, 13). The value of Mg# = Mg/(Mg + Fe) of these rocks ranges from 0.78 to 0.81, and the average Al_2O_3/TiO_2 and CaO/Al_2O_3 ratios are 12.27 and 1.23, respectively, which led us to ascribe them to the Al-depleted (Barberton) type of komatiites.

The MgO concentrations in the komatiite metabasalts (MgO < 18 wt %) are 11.53–17.39 wt % (Table 2, analyses 1, 2, 4, 5, 8, 10, 14 at Mg# = 0.64–0.77). A decrease in the Mg# value of the komatiite metabasalts is associated with an increase in the concentrations of CaO and Al_2O_3, which testifies to an increase in the contents of clinopyroxene and plagioclase in the melt (they have CaO/Al_2O_3 = 1.47–1.14 and Al_2O_3/TiO_2 = 13.0–13.39).

According to the configuration of their REE patterns, the metakomatiites and metakomatiite basalts are subdivided into two groups. The first group of the komatiites is characterized by weakly fractionated REE patterns close to chondritic ones [$(La/Yb)_N$ = 1.62–1.81] at weak depletion in HREE [$(Gd/Yb)_N$ = 1.43–2.13]. (Fig. 12a). The second group of komatiites is characterized by strongly fractionated REE patterns [$(La/Yb)_N$ = 15.9] (Fig. 12b) at notable enrichment in LREE [$(Ce/Yb)_N$ = 3] and depletion in HREE. The enrichment of LREE in the second-group komatiites can be explained by mantle metasomatism, which could occur locally shortly before the melting of the mantle source. The $(Gd/Yb)_N$ ratios of the two komatiite groups vary from 1.43 to 3.59 and confirm the conclusion, drawn from the petrochemical characteristics of the rocks, that the metakomatiites of the Dzhugdzhur Complex belong to the Barberton type [32].

It follows from the multielement diagram (Fig. 13) that the komatiites of the first group of the Dzhugdzhur Complex are enriched in Th, La, and Ce compared to the Phanerozoic komatiites of Gorgona Island [33]. Enrichment in these elements was also noted in the Early Archean komatiites of the Barberton greenstone belt [34]. This suggests that the Early Precambrian mantle beneath continents could be enriched in radioactive elements and LREE compared to the Phanerozoic mantle beneath the Pacific Ocean. This hypothesis was previously put forth in [35].

The komatiite basalts of both groups display an overall increase in REE concentrations. The contents of LREE in the metakomatiite basalt of the first group are 30 times higher than the chondritic values (Fig. 12a, sample E-17/174) and 600 times higher for the rocks of the second group (Fig. 12b, sample E-14/134).

As was demonstrated above, the metakomatiites of the Dzhugdzhur Complex affiliate with the Al-depleted type. This suggests that the residue of their parental melt contained garnet. The latter fact constrains the depth of the mantle magmatic chamber, according to the experimental data [36, 37], to approximately 200 km. The further ascent of the mantle plume with decreasing temperature and pressure, melting at depths shallower than 200 km should have occurred under olivine control.

It is difficult to constrain the thermodynamic parameters under which the parental melts of the metakomatiites were formed because of the effect of overprinted granulite metamorphism. These difficulties are caused by the obliteration of the original textural–structural features of the rocks and the absence of relict minerals. A principally important task is the determination of the noncumulus original composition of the komatiites. The use of melting diagrams for mantle lherzolites [38] and the relations between the MgO concentrations (wt %) of the metakomatiites and their Mg# values testify that the samples whose composition corresponds to that of the parental melt are 2107-A and E-17/160 (Table 2,

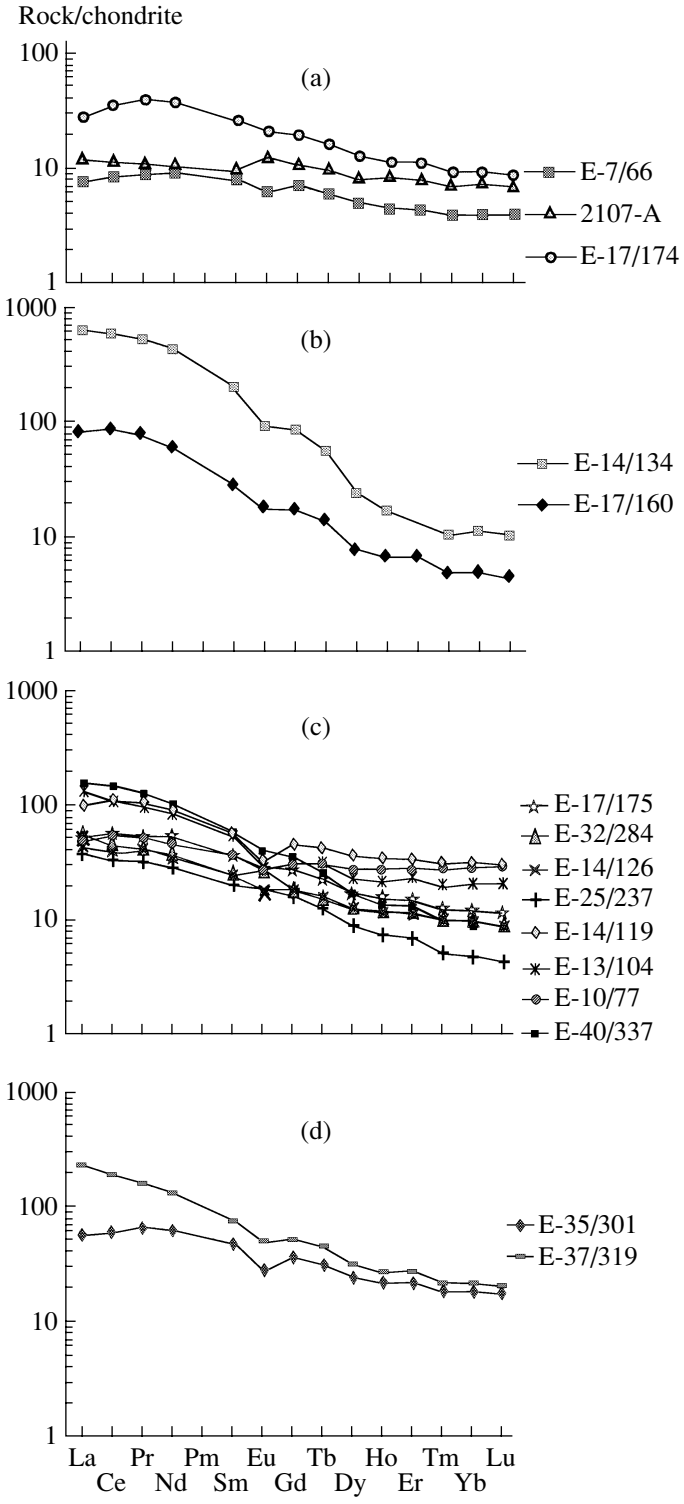

Fig. 12. Chondrite-normalized [21] REE patterns for the metavolcanic rocks of the komatiite–tholeiite series of the Dzhugdzhur granulite complex.

(a) Metakomatiites (2107-A and E-7/66) and komatiite metabasalt (E-17/174) of group I; (b) komatiite (E-17/160) and komatiite metabasalt of group II; (c) tholeiite metabasalts; (d) picrite metabasalts.

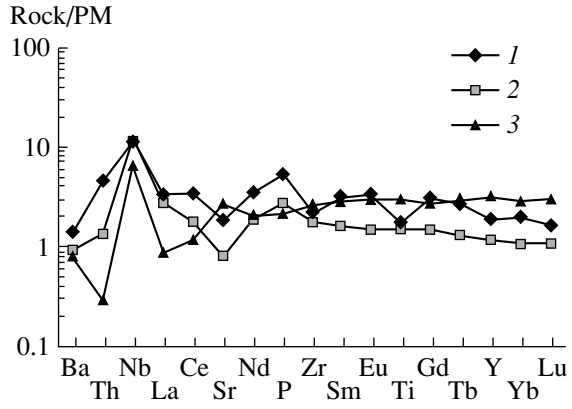

Fig. 13. Multielement diagram normalized to the primitive mantle [25] for metakomatiites of group I of the Dzhugdzhur Complex. (*1*) Metakomatiites of the Dzhugdzhur Complex; (*2*) komatiites of the Archean Barberton greenstone belt [32]; (3) Cretaceous komatiites of Gorgona Island in the Pacific Ocean [33].

analyses 7, 11), whereas the parental magma of sample E-7/66 contained much cumulus olivine.

Using the melting diagrams for mantle lherzolites [38], one can roughly evaluate the thermodynamic parameters at which the parental komatiite melts of the Dzhugdzhur Complex were formed: P = 32 kbar, T = 1530°C, degree of partial melting equal to 27%, with olivine and orthopyroxene as residue minerals for sample 2107-A (Table 2, analysis 7, 22.10 wt % MgO, Mg# = 0.78).

For sample E-17/160 (Table 2 analysis 11; 24.3 wt % MgO, Mg# = 0.8), these are P = 30 kbar, T = 1560°C, degree of partial melting equal to 39%; the residue minerals are olivine and orthopyroxene.

Still lower P-T parameters were determined for the parental melts of the komatiite basalts. For example, the following parameters were determined (using the aforementioned diagrams) for sample E-17/174 of komatiite metabasalt (Table 2, analysis 10; 17.39 wt % MgO, Mg# = 0.77): P = 18 kbar, T = 1250°C, degree of partial melting equal to 25%; the residue minerals are olivine, orthopyroxene, and clinopyroxene. Our data validate the model for the derivation of the parental high-Mg lavas of the Dzhugdzhur Complex by the partial decompression-induced melting of an ascending mantle plume. Experimental data and thermodynamic simulations [38, 39] indicate that less magnesian parental melts, including those of the tholeiitic basalts of the Dzhugdzhur Complex, could be formed by the fractionation of high-Mg komatiite basalts in intermediate relatively shallow chambers.

Metabasalts of the picrite series

The metabasalts of the picrite series gave rise to orthopyroxene–clinopyroxene schists, whose petrography is practically identical to that of the orthopyrox-

Table 3. Sm–Nd isotopic data on orthopyroxene–clinopyroxene schists of the Dzhugdzhur Complex

Sample	Nd (ppm)	Sm (ppm)	$^{143}Nd/^{144}Nd$	$^{147}Sm/^{144}Nd$	$T_{(DM)}$	$\varepsilon_{Nd}T$
E-17/158	26.38	5.45	0.511772	0.1248	2356	5.30
E-17/159	43.13	7.77	0.511566	0.1089	2298	6.18
E-35/296	16.96	3.28	0.511435	0.1169	2689	1.15

Note: The Sm and Nd isotopic measurements were conducted by G.M. Vovna under the supervision of Prof. D. Maeda on a Finnigan MAT-262 multicollector mass spectrometer at the Hokkaido University in Sapporo, Japan. The ε_{Nd} T values were calculated for T 2400 Ma.

ene–clinopyroxene schists that were described above and correspond to komatiite metabasalts. They were recognized on the basis of petrochemical features in the diagram (Fig. 11). Their distribution and abundances have not been quantified. Judging from their insignificant amounts in our collection of samples selected during the fieldwork, their amount is much smaller than that of the tholeiitic metabasalts.

The picrite metabasalts differ from the komatiite metabasalts in having higher concentrations of TiO_2 (1.23–2 wt %) at equal contents of MgO and, because of this, lower Al_2O_3/TiO_2 ratios. This allowed us to identify them in the discriminant diagram (Fig. 11). The metabasalts of the picrite series contain 5.18–13.1 wt % MgO (Table 2, analyses 3, 9) at Mg# = 0.47–0.68. The average CaO/Al_2O_3, CaO/TiO_2, and Al_2O_3/TiO_2 ratios are 0.88, 8.03, and 9.25, respectively. As can be seen from these values, the basalts of the picrite series have lower values of the CaO/TiO_2 and Al_2O_3/TiO_2 ratios.

The REE patterns of the picrite low-Si varieties of the metabasalts are weakly differentiated. For example, sample E-35/301 (46.06 wt % SiO_2) has $(La/Yb)_N = 3$ (Fig. 12d). An increase in the SiO_2 concentration is associated with an increase in the overall REE contents, particularly those of LREE. For example, sample E-37/319 (50.72 wt % SiO_2) has a $(La/Yb)_N$ ratio equal to 10 (Fig. 12d).

The genesis of the volcanics of the picrite series of normal alkalinity can, in principle, be explained within the scope of the same model as that proposed above for the komatiite–tholeiite series [40]. It is reasonable to believe that the low-Mg picrite basalts identified among the protolithic volcanics of the Dzhugdzhur Complex were formed by the crystallization differentiation of picrites in intermediate shallow-sitting chambers. However, the thermodynamic parameters at which the parental picrite magma was derived remain uncertain because our collection contains no rocks corresponding to these picrites. It can be hypothesized that the magmatic source of these picrites was the same mantle plume as for the komatiites. However, the picrite melts were derived at lower degrees of partial melting than those of the komatiite melts [40].

Sm–Nd Systematics of Rocks of the Metabasite–Enderbite Association

The Sm–Nd studies of the rocks of the metabasite–enderbite association were carried out for the orthopyroxene–clinopyroxene schists compositionally approximating basaltic andesites. The chemical compositions of these schists are shown in Table 1. The results of our Sm–Nd isotopic studies are summarized in Table 3. The $T_{(DM)}$ values obtained for the rocks led us to date the origin of their protoliths at the Early Proterozoic.

The positive $\varepsilon_{Nd}T$ values testify that the melts of the basaltic andesites of the basalt–andesite association were derived from depleted basites.

CONCLUSIONS

The results of our research led us to the following conclusions. The deep-seated granulite complex of the Dzhugdzhur block, which consists, according to petrological data, of lower crustal rocks, comprises two units. Their protoliths were volcanic and volcanic–sedimentary rocks for the lower and upper units, respectively. The lower unit consisted of volcanic rocks of three petrochemical series: calc–alkaline, komatiite–tholeiite, and picrite. The protolithic volcanics of these series were derived from different sources and were erupted roughly simultaneously onto the surface before the metamorphic event, as follows from their intercalation within a single stratigraphic sequence.

The models proposed for the genesis of the rocks of the komatiite–basalt, picrite, and calc–alkaline series make it possible to develop an integral model for all magmatic protoliths of the Dzhugdzhur Complex. In our opinion, this model comprises two stages. The first of them includes the initial ascent of a mantle plume and its decompression partial melting. The Al-depleted composition of the metakomatiites indicates that the mantle plume was generated at a depth of more than

200 km. The further ascent of the mantle plume was associated with the separation of picrite and komatiite melts from it at depths of approximately 100 km and komatiite basalts at depths of 50–60 km (see above). The differentiation of komatiite basalt in intermediate chambers at shallow depths gave rise to tholeiitic basalts. The second stage included the derivation of volcanic rocks of the calc–alkaline series via the partial melting of older basite crustal material. The geochemistry of these basites is thought to have been close to that of the protolithic tholeiites of the neighboring Sutam block of the Aldan Shield. This tholeiite magmatism occurred in the southern part of the Aldan Shield at 3.1 Ga and caused the underplating of the preexisting Early Archean basite crust. The metamorphism and subsequent melting of this basite crust were induced by the heat of melts that separated from the plume and by the general ascent of geotherms associated with plume ascent. Various degrees of melting of this crust formed the parental melts of the basalt, basaltic andesite, and andesite compositions of the calc–alkaline series of the Dzhugdzhur Complex.

The lower unit is dominated (up to 60% by volume) by hypersthene plagiogneisses (enderbites) of andesite composition, with the rest of the unit consisting of basaltic andesites and basalts with minor amounts of ultrabasic volcanic rocks. Our data provide insight into the composition of the lowermost crustal levels in the southeastern part of the Aldan Shield. We also obtained the first Sm–Nd isotopic data testifying to the Early Proterozoic age of the protoliths of the metabasite–enderbite association, which notably modifies the preexisting concepts of both the age of the Dzhugdzhur block and its geotectonic setting (the position of the southeastern boundary of the Aldan Shield and the recognition of an Early Proterozoic folded area, whose fragment could be the Dzhugdzhur block).

REFERENCES

1. A. A. Marakushev, *Problems of Mineral Facies of Metamorphic and Metasomatic Rocks* (Nauka, Moscow, 1965) [in Russian].
2. L. L. Perchuk, I. V. Lavrent'eva, L. Ya. Aranovich, and K. K. Podlesskii, *Biotite–Garnet–Cordierite Equilibria and Metamorphic Evolution* (Nauka, Moscow, 1983) [in Russian].
3. O. V. Avchenko, *Mineral Equilibria in the Metamorphic Rocks and Geobarometric Problems* (Nauka, Moscow, 1990) [in Russian].
4. L. Ya. Aranovich, *Mineral Equilibria of Multicomponent Solid Solutions* (Nauka, Moscow, 1991) [in Russian].
5. A. B. Kotov, Extended Abstract of Doctoral Dissertation in Geology and Mineralogy (St. Petersburg, 2003).
6. *Geological Map of the USSR. Scale 1 : 200000. Sheet N-52-VI* (Moscow, 1969) [in Russian].
7. *Geological Map of the USSR. Scale 1 : 200000. Sheet N-53-I* (Moscow, 1969) [in Russian].
8. V. N. Moshkin, Extended Abstract of Candidate's Dissertation in Geology and Mineralogy (Leningrad, 1962).
9. Yu. N. Gamaleya, "Formation Analysis and Evolution of the Southeastern Siberian Platform in the Precambrian," Geotektonika, No. 6, 34–45 (1968).
10. M. K. Sukhanov and D. Z. Zhuravlev, "Sm–Nd Dating of Dzhugdzhur Anorthosites," Dokl. Akad. Nauk SSSR **304** (4), 964–968 (1989).
11. V. N. Moshkin and I. N. Dagelaiskaya, "Anorthosite Association," in *Magmatic Rock Associations of USSR* (Nedra, Leningrad, 1979) [in Russian].
12. L. A. Neimark, A. M. Larin, G. V. Ovchinnikova, and S. Z. Yakovleva, "U–Pb Age of the Dzhugdzhur Anorthosites," Dokl. Akad. Nauk SSSR **323** (3), 514–518 (1992).
13. G. P. Sighinolfi, "Investigation Into Deep Crustal Levels: Fractionating Effects and Geochemical Trends Related to High-Grade Metamorphism," Geochim. Cosmochim. Acta **35** (10), 1005–1021 (1971).
14. K. C. Condie and P. Allen, "Origin of Charnockites from Southern India," in *Archean Geochemistry*, Ed. by A. Kroner, G. N. Hanson, and A. M. Goodwin (Springer-Verlag, Berlin-Heidelberg, 1984; Mir, Moscow, 1987), pp. 182–203.
15. S. S. Sun and R. W. Nesbitt, "Petrogenesis of Archaean Ultrabasic and Basic Volcanics: Evidence from Rare Earth Elements," Contrib. Mineral. Petrol. **65** (3), 301–325 (1978).
16. W. H. Dennen and B. R. Moore, "Chemical Definition of Nature Detrital Sedimentary Rock," Nat. Phys. Sci. **234**, 127–128 (1971).
17. *Classification of Magmatic (Igneous) Rocks and Vocabulary of Terms* (Nedra, Moscow, 1997), p. 248 [in Russian].
18. M. A. Mishkin, *Metamorphism in the Asia–Pacific Ocean Transition Zone* (Nauka, Moscow, 1981) [in Russian].
19. L. A. Winchester and P. A. Floyd, "Geochemical Discrimination of Different Magma Series and Their Differentiation Products Using Immobile Elements," Chem. Geol. **20** (4), 325–343 (1977).
20. L. S. Jensen, "A New Cation Plot for Classifying Subalkalic Volcanic Rocks," Ontario Div. Mines. Misc. P, 66 (1976).
21. N. M. Evensen, P. J. Hamilton, and R. K. O' Nions, "Rare Earth Elements Abundances in Chondritic Meteorites," Geochim. Cosmochim. Acta **42** (8), 1199–1212 (1978).
22. K. Condie, *Archaen Greenstone Belts* (Elsevier, Amsterdam, 1981; Mir, Moscow, 1983) [in Russian].
23. T. I. Frolova and I. A. Burikova, *Magmatic Rock Associations of the Modern Geodynamic Settings* (Mosk. Gos. Univ., Moscow, 1997) [in Russian].
24. H. Martin, "The Archean Grey Gneisses and the Genesis of Continental Crust," in *Arhean Crustal Evolution*, Ed. by K. C. Condie (Elsevier, Amsterdam, 1994), pp. 205–259.
25. R. Rollinson, *Using Geochemical Data: Evaluation, Presentation, Interpretation* (Longman Scientific and Technical, London, 1993).
26. M. B. Wolf and P. J. Willey, "Some Results of Experimental Study of Dehydration Amphibolite Melting at 10 kbar," Geol. Geofiz., No. 12, 100–115 (1993).

27. D. M. Shaw, "Trace Element Fractionation during Anatexis," Geochim. Cosmochim. Acta **34** (2), 331–340 (1970).
28. M. A. Mishkin, G. M. Vovna, S. N. Lavrik, and R. A. Oktyabr'skii, "Geochemistry and Genesis of Deep-Seated Archean Enderbites in the Sutam Block, Southern Aldan Shield," Geokhimiya, No. 7, 691–711 (2001) [Geochem. Int. **39**, 627–645 (2001)].
29. A. W. Hofman, "Chemical Differentiation of the Earth: The Relationship Between Mantle, Continental Crust, and Oceanic Crust," Earth Planet. Sci. Lett. **90** (3), 297–314 (1988).
30. G. A. Avdeiko, A. Yu. Antonov, O. N. Volynets, et al., *Submarine Volcanism and Zoning of the Kurile Island Arc* (Nauka, Moscow, 1992) [in Russian].
31. V. S. Kulikov and V. V. Kulikova, "A New Approach to the Classification of High-Magnesian Rocks," in *Proceedings of the 2nd All-Russia Petrographic Conference* (Syktyvkar, 2000), Vol. 1, pp. 111–112 [in Russian].
32. R. W. Nesbitt, Bor-Ming Jahn, and A. C. Purvis, "Komatiites: An Early Precambrian Phenomenon," J. Volcanol. Geotherm. Res. **14**, 31–45 (1982).
33. A. C. Kerr, G. F. Marriner, N. T. Arndt, et al., "The Petrogenesis of Gorgona Komatiites, Picrites and Basalts: New Field, Petrographic and Geochemical Constraints," Lithos **37**, 245–260 (1996).
34. K. P. Jochum, N. T. Arndt, and A. W. Hofman, "Nb–Th–La in Komatiites and Basalts: Constraints on Komatiite Petrogenesis and Mantle Evolution," Earth Planet. Sci. Lett. **107**, 272–289 (1991).
35. M. A. Mishkin and G. M. Vovna, "Early Sialic Crust of the Continental Framing of the Pacific Ocean," in *Geological Structure and Origin of the Pacific Ocean* (Dal'nauka, Vladivostok, 2005), pp. 85–98 [in Russian].
36. M. I. Bickle, C. E. Ford, and E. A. Nisbet, "The Petrogenesis of Peridotitic Komatiites: Evidence from High Pressure Melting Experiments," Earth Planet. Sci. Lett. **37**, 97–106 (1997).
37. E. Ohtani, I. Kawabe, I. Moriyama, et al., "Partitioning of Elements Between Majorite Garnet and Melt and Implications for Petrogenesis of Komatiite," Contrib. Mineral. Petrol. **103**, 263–269 (1989).
38. I. D. Ryabchikov and O. A. Bogatikov, "Physicochemical Conditions of Generation and Differentiation of the Karelian Komatiites," Geokhimiya, No. 5, 645–638 (1984).
39. A. V. Girnis, I. D. Ryabchikov, and O. A. Bogatikov, *Genesis of Komatiites and Komatiitic Basalts* (Nauka, Moscow, 1987) [in Russian].
40. *Magmatic Rocks*, Ed. by O. A. Bogatikov (Nauka, Moscow, 1987) [in Russian].